Tyre/road noise: A piston approach for CFD modeling of air volume variation in a cylindrical road cavity

Marianne Bou Leba Bassil, Julien Cesbron, Philippe Klein

Journal Pre-proof

Tyre/road noise: A piston approach for CFD modeling of air volume variation in a cylindrical road cavity

Marianne Bou Leba Bassil, Julien Cesbron, Philippe Klein

PII: S0022-460X(19)30703-5

DOI: https://doi.org/10.1016/j.jsv.2019.115140

Reference: YJSVI 115140

To appear in: *Journal of Sound and Vibration*

Received Date: 26 June 2019

Revised Date: 4 November 2019

Accepted Date: 6 December 2019

Please cite this article as: M.B.L. Bassil, J. Cesbron, P. Klein, Tyre/road noise: A piston approach for CFD modeling of air volume variation in a cylindrical road cavity, *Journal of Sound and Vibration* (2020), doi: https://doi.org/10.1016/j.jsv.2019.115140.

Tyre/road noise: a piston approach for CFD modeling of air volume variation in a cylindrical road cavity

Marianne Bou Leba Bassil*

IFSTTAR, CEREMA, UMRAE, F-44344 Bouguenais, France

Julien Cesbron

IFSTTAR, CEREMA, UMRAE, F-44344 Bouguenais, France

Philippe Klein

Univ. Lyon, IFSTTAR, CEREMA, UMRAE, F-69675, Lyon, France

Abstract

This paper deals with air volume variation in a road cavity during the rolling of a slick tyre leading to air-pumping. A numerical model was developed based on Computational Fluid Dynamics (CFD), coupled with a function representing the volume variation due to the tyre tread penetration inside the cavity. A simplified method based on an equivalent piston-like movement of the cavity bottom is derived from a tyre/road contact model and validated by comparison with a membrane approach. This method was used to conduct a parametric study to assess the influence of volume variation and rolling speed on dynamic air pressures and associated signal energy levels. It was found that the overpressure reached during the contact increases with the volume variation of the cavity and with the rolling speed. The pressure signal energy level emitted at the leading edge increases with the velocity but is negligibly influenced by the volume variation. However, the signal energy level at the trailing edge increases with the volume variation without being influenced by the rolling speed. Furthermore, the speed exponent linking the signal energy level with rolling speed was found to be less than 4 at the leading and trailing edges which is consistent with previous work.

*Corresponding author

Email address: marianne.bassil@ifsttar.fr (Marianne Bou Leba Bassil)

Keywords: tyre/road noise, air-pumping, Computational Fluid Dynamics, piston method, tyre/road contact, volume variation

1. Introduction

Environmental noise is a major issue affecting quality of life and health of millions of people [1]. One of the most annoying nuisances in densely populated areas is road traffic noise, which dominant contribution at steady speed flows above 40 km/h is tyre/road noise [2]. Early studies on tyre/road noise [3, 4] have revealed the existence of two main independent generating mechanisms: radial vibrations of the tyre structure dominate at low and medium frequency (below 1000 Hz) while air flow related mechanisms, often called air-pumping, generate noise at high frequency (above 1000 Hz). These generating mechanisms are fully described in [5] and can be accompanied in certain configurations by stick/slip or stick/snap phenomena and pipe or Helmholtz resonances. The resulting sources in the vicinity of the tyre are amplified by horn effect [6, 7] before propagation at the road side.

Vibratory and aerodynamic sources lead to different speed exponent k when considering the relationship between squared acoustic pressure and rolling speed for both kinds of contribution. Most previous work [3, 8] led to a value of k between 2 and 3 for vibratory mechanisms dominating at low frequency and a value between 4 and 5 for aerodynamic mechanisms at high frequency. However, a statistical analysis on a large tyre/road noise database [9] showed a dominance of vibratory mechanisms over the entire range of frequencies. Further analysis in [10] has highlighted the contribution of air-flow related mechanisms in the generation of noise even in the low frequency range. Thus the separation of both mechanisms remains unclear and further investigation are needed, especially on air-pumping phenomena. Indeed a recent literature review on tyre-road interaction noise [11] clearly shows the gap between the number of studies on tyre vibrations and those on air-flow related mechanisms. Therefore, this paper aims at further insight on air-pumping in the case of a tyre rolling on a cylindrical cavity incorporated in the road and its contribution to noise generation.

Air-pumping is often defined as the series of rapid air compressions and releases at the interface between the tyre and the road during rolling. Two kinds of phenomena have been investigated to explain the origin of air pressure fluctuations. A first category of studies [12, 13, 14] have shown that the

viscous boundary layer at the tyre and road surfaces contributes to the generation of pressure fluctuations. In a second category of studies, air-pumping was attributed to air volume variation due to tyre tread deformation in the contact patch, which may have different origins. It can be firstly favored by deformation of grooves and cavities on the tread pattern, then by indentation of road asperities and finally by rubber penetration in cavities incorporated in the road surface.

On the one hand, the effect of tread patterns on noise emission has been widely studied experimentally [15, 16] and analytically [17, 18, 19]. Further numerical methods based on Computational Fluid Dynamics (CFD) have been conducted in order to study tyre grooves effect on air-pumping. A three-stage hybrid technique that combines CFD with Kirchhoff integral was developed by Kim et al. [20] in order to calculate air flow properties and acoustic pressure. The 3D model simulated the deformation of a tyre transverse groove on a pavement based on a piston/sliding door/cavity model. Fabrizi [21] investigated noise generation mechanisms of the pipe resonance phenomenon with CFD (Fluent Large Eddy Simulation (LES) model) and computational aeroacoustics (Ffwocs William-Hawking (FW-H) model). The model represents a commercial tyre having a single longitudinal groove and enveloped by an air flow with an inlet velocity. In the same context, Gautam and Chandy [22] carried out numerical simulations of air-pumping in a 2D tyre transverse groove. The groove deformation was taken into account by two methods: the first one uses a piston-like motion of the bottom wall and the second method is the deformation of the side walls of the groove that gradually bulge inward and outward as the groove moves in and out of the contact patch. A comparative study was conducted to examine the impact of the deformation model on air-pumping and noise generation at the small scale using LES turbulence model in Fluent. This approach was proceeded in 3D [23] for a cylinder with two transverse grooves in the circumferential direction. Simulations of air-pumping were conducted with the LES and noise estimated with FW-H models.

On the other hand, little research has been performed on the effect of air volume variation due to rubber indentation by road asperities or its penetration in road cavities during rolling. Road asperities were analytically modeled by Ronneberger [24] to simulate rubber indentation during rolling. It was shown that air-pumping originates from the tread deformation during its impact with the road surface, which forces air to be expelled or sucked into the outside/inside of the cavities. In some way, the effect of rubber pen-

etration in a road cavity on air-pumping was indirectly investigated by the experiment of Hamet et al. [25]. In this work, a slick tyre was rolling on a cylindrical cavity incorporated in the road. An overpressure at the bottom of the cavity was observed during its obturation by the tyre, followed by a pressure drop at the opening and a Helmholtz-like resonance. This phenomenon was qualitatively reproduced by Conte and Jean [13] with CFD simulations only considering the viscous boundary layer effect. However, neglecting volume variation due to rubber penetration led to an underestimation of the overpressure in comparison with experimental results.

This paper aims at filling this gap and at highlighting the influence of volume variation due to tyre tread penetration into the cavity on air-pumping. Volume variation is modeled by a simplified piston-like motion of the cavity bottom which is firstly introduced in the paper. The piston approach is then validated by comparison with a membrane method that represents the tyre tread penetration at the top of the cavity. Due to technical difficulties in implementing the membrane approach in 3D, the CFD model is here implemented in 2D, but the piston approach could be generalized in 3D for more complex geometries. Subsequently, a parametric study is performed to evaluate the influence of volume variation and rolling speed on air pressure fluctuations at the tyre/road interface. Finally, the impact of volume variation on the pressure signal energy level is assessed at the leading and trailing edges.

2. Piston method

The volume variation caused by the tyre tread penetration inside the road cavity during rolling is modeled by a simplified piston method. This approach is schematized in Figure 1. During the passage over the contact zone, the penetration of rubber in the cavity leads to a volume decrease (Figure 1 (a)) which can be equivalently described by a piston-like vertical displacement of the cavity bottom (Figure 1 (b)). It is thus considered that the cavity bottom moves vertically upward as the cavity closes. The maximum displacement is reached when the cavity is completely closed. Then the cavity bottom moves down symmetrically when the cavity opens.

The diagram in Figure 3 summarizes the whole procedure of the piston method. The first step is to use a contact model to get the overall geometry of the deformed tyre and the local penetration $z_m(x,t)$ of the tyre tread inside of the cavity (see Figure 1 (a)). The second step is to calculate the

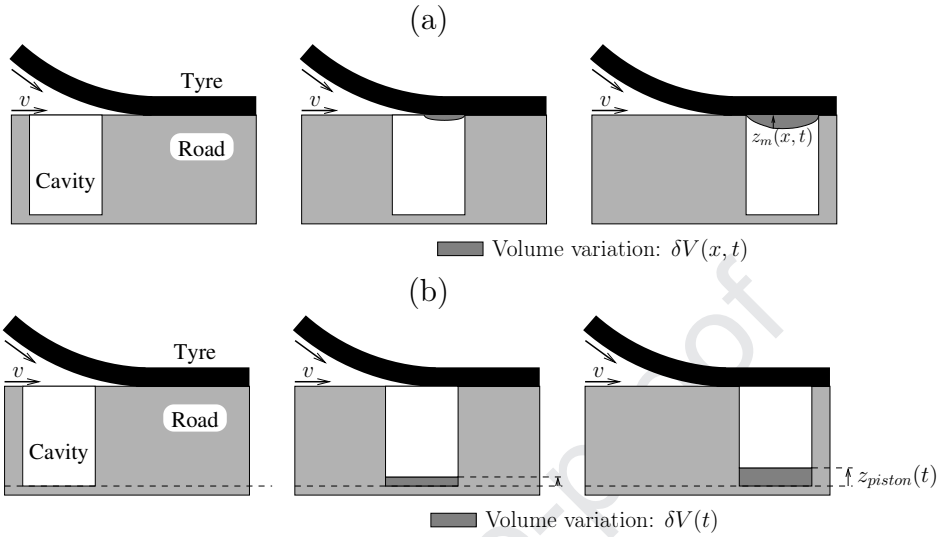

Figure 1: Volume variation of the cavity due to penetration of the tyre tread (a) and equivalent piston-like displacement of the cavity bottom (b)

volume variation of the cavity at each time step, leading to the equivalent displacement of the cavity bottom $z_{\text{piston}}(t)$ (see Figure 1 (b)). The last step is to perform a CFD calculation into the Fluent solver where the overall geometry of the deformed tyre and the piston model have been introduced.

For the sake of physical validation, the piston method has already been investigated by the authors in [26] and compared with the experimental results of Hamet et al. [25]. Contrary to the case without volume variation previously studied in [13], the piston method in 3D has led to a fairly good agreement with the pressure signal measured at the bottom of the cavity in [25], not only in shape but also in amplitude (Figure 2). However, on the one hand, it has to be noticed that the piston displacement was approximated by an arbitrary Tukey window function similar in shape to the pressure signal. On the other hand, the volume variation and the associated maximum displacement were estimated from the classical thermodynamic Laplace's law, by comparison between the measured pressure and the pressure calculated without volume variation. Having regard to the efficiency of the piston method, it would be interesting to directly calculate the actual volume variation instead of estimating it. Hence the purpose of the present paper that uses a contact model for calculating the tyre tread penetration in the road cavity prior using the piston method in the CFD calculation.

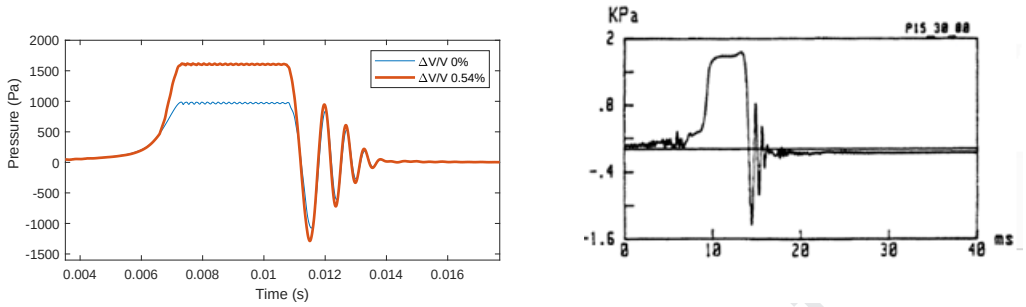

a) b)

Figure 2: a) Calculated pressure at the bottom of the cavity from a 3D model with and without volume variation [26] and b) Pressure signal measured by Hamet et al. [25]

The CFD numerical resolution of the problem enables the calculation of the flow properties such as air dynamic pressure at each time step. In this paper, the idea would be to check if the calculated air pressure (at the bottom of the cavity for example) obtained with this simplified piston method is close to that calculated by directly introducing the penetration of the tyre tread (noted as the membrane method). In the following, the theoretical background and hypotheses of the three above mentioned steps are presented.

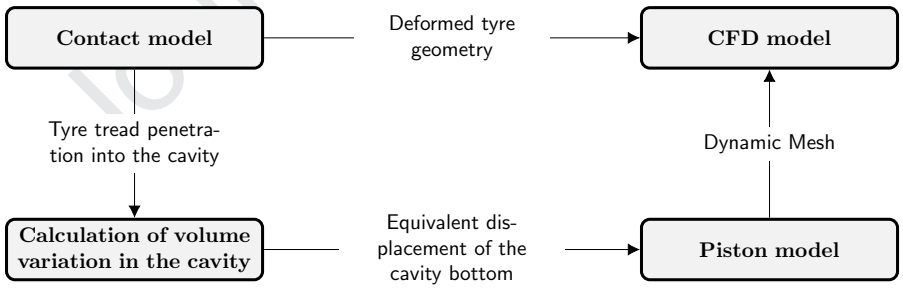

Figure 3: Principle of calculating the dynamic air pressure at the bottom of the cavity using the CFD model with volume variation (piston movement)

2.1. Contact model

In this part, a theoretical description of the contact model is presented. This model is used to calculate the overall deformed shape of the tyre as

well as its local deformation represented by the penetration of the tyre tread (membrane) inside the cavity. The road surface is considered as perfectly rigid and flat. For the sake of validation, the tyre structure is here simplified and modeled by an elastic half-space, but a more complex approach (e.g. FEM) would be possible. The contact problem is considered as a succession of static prints without friction and is described in Cartesian coordinates (x, y, z).

Under these assumptions, the Boussinesq's theory [27] applies and the relationship between the normal displacement u_z and the pressure distribution f_z at the surface of the half-space is given by :

$$\forall M \in \Sigma(t),\ u_z(M,t) = \int_{\Sigma_c(t)} G(M,S) f_z(S,t) dS \tag{1}$$

where Σ is the whole surface of the half-space, Σ_c is the contact area and $G(M,S)$ is the influence function of Boussinesq expressed as follows:

$$G(M,S) = \frac{1}{\pi E^* r} \tag{2}$$

with $r = \sqrt{(x_M - x_S)^2 + (y_M - y_S)^2}$ the distance separating the two points M and S in the (x, y) plane and $E^* = E/(1-\nu^2)$, where E is the Young's modulus and ν the Poisson's ratio of the elastic material.

The contact between the tyre and the road is sketched in Figure 4, where δ is the overall displacement at the wheel center, z_r^0 describes the undeformed surface of the road and z_t^0 the undeformed surface of the tyre. The unilateral contact conditions are expressed by :

$$\begin{cases} \forall M \in \bar{\Sigma}_c(t), & h(M,t) > 0 \quad \text{and} \quad f_z(M,t) = 0 & \textit{Separation} \\ \forall M \in \Sigma_c(t), & h(M,t) = 0 \quad \text{and} \quad f_z(M,t) > 0 & \textit{Contact} \end{cases} \tag{3}$$

where $\bar{\Sigma}_c$ represents the set of points that do not belong to the contact area at time t and the so-called gap function h describes the distance between the deformed tyre surface and the road surface:

$$h(M,t) = u_z(M,t) - z_r^0(M,t) + \delta(t) + z_t^0(M,t). \tag{4}$$

The resultant total load F_z satisfies the equilibrium equation:

$$F_z(t) = \int_{\Sigma_c(t)} f_z(S,t) dS \tag{5}$$

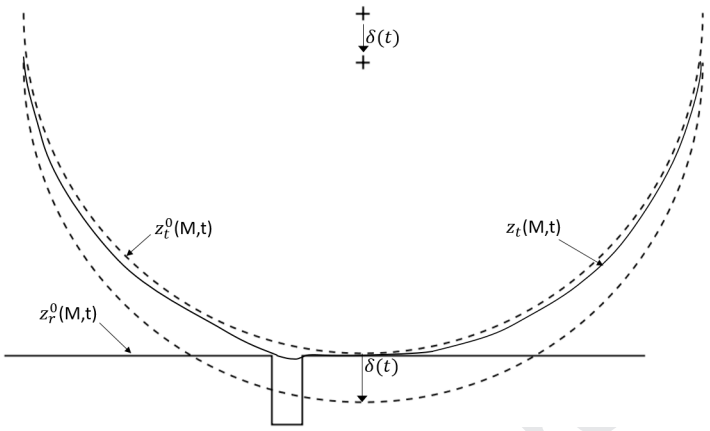

Figure 4: Geometric description of the contact at the pneumatic / road interface

and the deformed shape of the tyre surface z_t is given by:

$$z_t(M,t) = z_t^0(M,t) + u_z(M,t) + \delta(t) \tag{6}$$

2.2. Calculation of air volume variation in the cavity

In order to calculate the air volume variation in the cavity, this latter of diameter d and of depth L_0 is introduced into the geometry of the road surface z_r^0 by the following relation:

$$z_r^0(x,y,t) = \begin{cases} -L_0 & \text{if } \sqrt{(x-x_c(t))^2 + (y-y_c(t))^2} < d/2 \\ 0 & \text{if } \sqrt{(x-x_c(t))^2 + (y-y_c(t))^2} \geq d/2 \end{cases} \tag{7}$$

where $x_c(t)$ and $y_c(t)$ are the positions of the cavity center according to x and y given as follows:

$$\begin{cases} x_c(t) = vt + x_c(0) \\ y_c(t) = 0 \end{cases} \tag{8}$$

with v the rolling speed. The rolling of the tyre on the cavity is obtained by changing the position of the cavity center x_c with respect to the center of the tyre. A succession of static contacts is thus obtained, representing the deformed tread penetrating into the cavity.

Defining the set $\mathcal{C}(t)$ by:

$$\mathcal{C}(t) = \{M(x,y) \setminus \sqrt{(x - x_c(t))^2 + (y - y_c(t))^2} \leq d/2\}, \tag{9}$$

then the membrane displacement $z_m(M,t)$ is defined by:

$$\forall t, \forall (x,y) \in \mathcal{C}(t) \setminus z_t(M,t) \leq 0, z_m(M,t) = z_t(M,t) \tag{10}$$

where $z_t(M,t)$ is the deformed surface of the tyre given by Eq.(6).

Since the CFD simulations of the membrane penetration considered in this paper will be in 2D, $z_m(M,t)$ is noted as $z_m(x,t)$ corresponding to the penetration of the membrane into the cavity along the x axis (with $y = 0$) at time t. The set of points $z_m(x,t)$ is then stored for each cavity position in order to be coupled with the CFD model when applying the membrane method (see section 3.2). Time t is obtained from the distance D traveled by the cavity by the simple relation $t = D/v$.

Then, for the simplified piston method, the membrane displacement $z_m(M,t)$ is used to calculate the equivalent volume of the tread penetrating into the cavity:

$$v_p(t) = \int\limits_{\Sigma_c(t)} z_m(M,t) dM \tag{11}$$

In 2D, the equivalent surface penetrating into the cavity is given by:

$$s_p(t) = \int\limits_{\Sigma_c(t)} z_m(x,t) dx \tag{12}$$

In 3D, it is assumed that the volume of penetration into the cavity $v_p(t)$ is equivalent to a cylindrical volume swept by the piston movement of the cavity bottom. The equivalent displacement of the cavity bottom $z_{\text{piston}}(t)$ is thus calculated as follows:

$$z_{\text{piston}}(t) = \frac{4 v_p(t)}{\pi d^2} \tag{13}$$

In 2D, the surface of penetration into the cavity $s_p(t)$ is equivalent to a rectangular surface swept by the piston movement of the cavity bottom. The equivalent displacement of the cavity bottom $z_{\text{piston}}(t)$ is calculated as follows by:

$$z_{\text{piston}}(t) = \frac{s_p(t)}{d} \tag{14}$$

The membrane displacement $z_m(x,t)$ and the equivalent piston displacement $z_{\text{piston}}(t)$ are then used in the CFD model in order to calculate the air dynamic pressure variation resulting from the air volume variation of the cavity during rolling with respect to the dynamic pressure induced by viscous boundary layer effect only. The theoretical description of the CFD model is given in the following.

2.3. CFD model

Solving fluid dynamics problem requires the calculation of various flow properties such as velocity, density, pressure and temperature as functions of space and time. Although the tyre rolling process implies low Mach number, the fluid is considered compressible to enable capturing of generated acoustic waves. The equations that govern the fluid motion are the Navier-Stokes equations and its derivatives. These are nonlinear partial differential equations corresponding to conservation laws for mass, momentum and energy.

The conservation of mass is expressed as follows:

$$\frac{\partial \rho}{\partial t} + \text{div}\ (\rho \mathbf{V}) = 0 \tag{15}$$

where ρ is the density and $\mathbf{V}$ is the velocity of a fluid particle.

The conservation of momentum is written as:

$$\frac{\partial (\rho \mathbf{V})}{\partial t} + \mathbf{div}\ (\rho \mathbf{V} \otimes \mathbf{V}) = \mathbf{div}\ \boldsymbol{\tau} - \mathbf{grad}\ p + \rho \mathbf{g} \tag{16}$$

where p and $\boldsymbol{\tau}$ represent respectively the thermodynamic pressure and the viscous terms of the stress tensor arising from the fluid motion, while $\mathbf{g}$ denotes body accelerations (e.g. gravity or inertial accelerations). Here air is considered as a Newtonian fluid entailing a linear and isotropic relation between viscous stresses and strain rate. Assuming Stokes hypothesis (volume viscosity is neglected), $\boldsymbol{\tau}$ can be expressed as:

$$\boldsymbol{\tau} = \mu \left(\mathbf{grad}\mathbf{V}^T + \mathbf{grad}\mathbf{V} \right) - \frac{2}{3}\mu (\text{div}\mathbf{V})\mathbf{I} \tag{17}$$

where μ is the fluid dynamic viscosity and $\mathbf{I}$ is the unit tensor.

The conservation of energy is expressed assuming airflow without radiation as:

$$\frac{\partial (\rho E)}{\partial t} + \text{div}\ (\rho E \mathbf{V}) = -\mathbf{grad}\ p\mathbf{V} + \text{div}\ (\boldsymbol{\tau} \overline{\otimes} \mathbf{V}) + \rho\ \mathbf{g} \overline{\otimes} \mathbf{V} - \text{div}\mathbf{q} \tag{18}$$

where E is the total energy per unit mass and $\mathbf{q}$ the thermal flux proportional to temperature gradient according to Fourier's law of thermal conduction.

The ideal gas law connecting pressure, density and temperature T is added for closing the system of equations and writes

$$p = \rho \frac{R}{M} T \tag{19}$$

where R and M are the ideal gas constant and molar mass.

Given typical rolling speed and tyre size, air flow is assumed to be turbulent. However the dynamics of turbulent eddies is not studied here since its effect on air-pumping is considered negligible with respect to the average flow. Turbulent noise sources are not evaluated given the low speed considered. A statistical URANS (Unsteady Reynolds Average Navier-Stokes) approach is used to model the turbulent components and solve the average flow. The RANS model used to determine the unknowns introduced by the average of the Navier-Stokes equations is selected on the basis of its validity for solving the flow in the boundary layers which is a key point for the problem considered. Thus, air-pumping mechanism is directly captured by air dynamic pressure fluctuations.

The 2D model chosen for the numerical simulation is based on the work of Conte [13] dealing with a slick tyre rolling on a cylindrical cavity. Its general concept is represented in Figure 5.The origin of the reference frame and the calculation domain is chosen at the center of the wheel. The tyre rotates with an angular velocity ω while the cavity and the road are in translational motion with a velocity v along the x-axis.

It is shown in [13] by comparing 3D and 2D simulation results that in 3D (with a finite width tyre) the airflow has a rather low influence on the pressure fluctuations while in 2D (meaning an infinite width tyre) it produces a strong pressure difference between the leading edge and trailing edge leading to strongly biased results. Thus, direct air flow on the wheel is not considered in this case. It is only generated by the surface displacement and the development of corresponding boundary layers due to air viscosity. Unsteady conditions are generated by the translational motion and deformation of the cylindrical cavity according to previous section.

Non-Reflective Boundary Conditions (NRBC) are imposed at the domain boundaries to control spurious wave reflections. General NRBCs are derived by first recasting the Euler equations in an orthogonal coordinate system

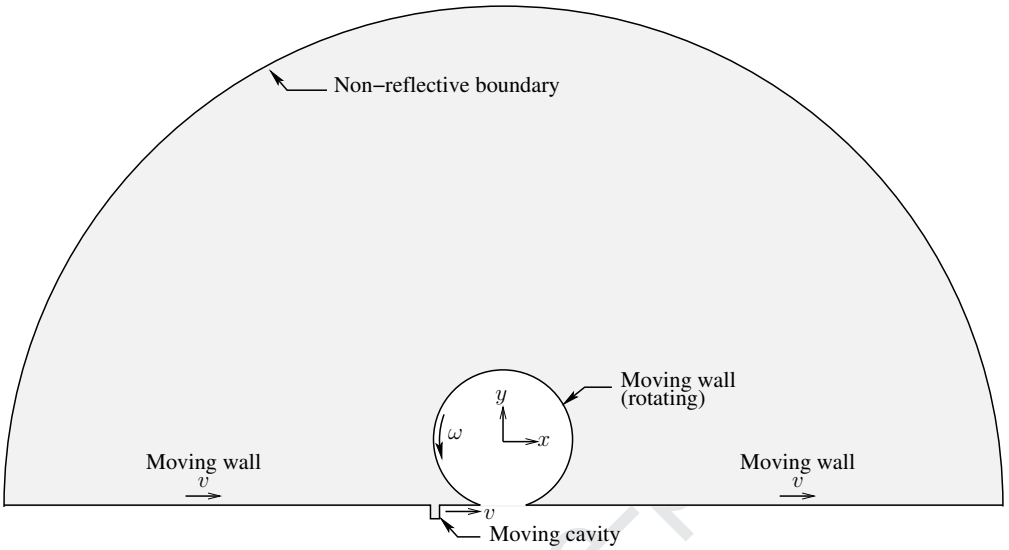

Figure 5: General concept of the CFD model of a rolling tyre on a cylindrical cavity

$(\mathbf{x_1}, \mathbf{x_2}, \mathbf{x_3})$ such that one of the coordinates, $\mathbf{x_1}$, is normal to the boundary. The characteristic analysis is then used to modify terms corresponding to waves propagating in the $\mathbf{x_1}$ normal direction. When doing so, a system of equations can be written to describe the wave propagation [28] and avoid reflection at limits of the domain.

3. Numerical implementation and validation of the piston method

For the sake of numerical implementation and validation of the piston method, the experimental configuration described in Hamet *et al.*[25] is considered. It consists of a slick tyre of diameter 631.4 mm rolling at 80 km/h ($22.2\,\mathrm{m\,s^{-1}}$) on a pavement with an incorporated cylindrical cavity of diameter $d = 15$ mm and depth $L_0 = 30$ mm. The solving methods of the contact model and the CFD model are explained in the following leading respectively to the calculation of cavity volume variation and air dynamic pressure at each time step.

3.1. Numerical implementation of the contact model

The tyre is modeled by an elastic half-space of Young's modulus $E = 6$ MPa and Poisson's ratio $\nu = 0.5$. The imposed normal load is $F_z = 4700$ N. The length of the contact patch along the rolling direction is 9 cm.

The contact problem is solved by the classical direct iterative method [29], the so-called Matrix Inversion Method (MIM). The numerical procedure is based on a prediction/correction algorithm fully detailed in [30], with an imposed normal load F_z.

The surface of the half-space is divided into n identical rectangular elements of dimensions h_x along x-axis and h_y along y-axis and centered around points M_i ($i \in [1, n]$) of coordinates (x_i, y_i) (Figure 6).

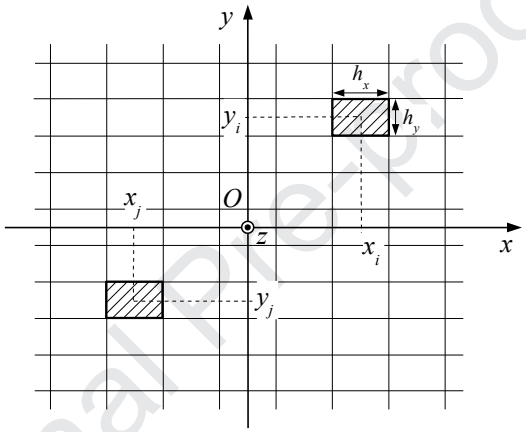

Figure 6: Discretization of the surface of the half-space [30]

Solving the contact problem leads to the calculation of the overall geometry of the deformed tyre as well as the local deformation of the tyre tread (penetration) into the cavity. The overall tyre deformed geometry is first used in a CFD model to create the fluid domain around the tyre. Then, the tread penetration into the cavity is used to deduce its volume variation (cf. Figure 3). Procedures for obtaining the two types of tyre deformation are explained in the following.

On the one hand, the resolution of the contact is performed on a rigid and smooth surface in order to obtain the overall geometry of the deformed tyre. The spatial resolution of the mesh according to x and y is fixed at $h_x = h_y = 3$ mm for tyre contact calculation on the smooth surface. Figure 7 shows the complete deformed tyre geometry, to be used in the CFD model.

On the other hand, the contact is performed on a flat surface with the incorporated cylindrical cavity in order to calculate the penetration of the

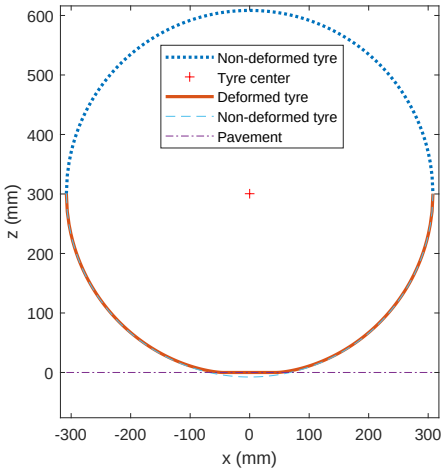

Figure 7: Deformed tyre obtained by the tyre/road contact model

tread in the cavity during the passage of the tyre. In this case the mesh resolution is fixed to $h_x = h_y = 1$ mm. Figure 8a gives the contact pressure distribution when the wheel center is aligned with the cavity center and Figure 8b shows the corresponding penetrating of the tread in the cavity. Examples on the tyre tread penetration obtained for different locations of the cavity center relative to the wheel center are shown in Figure 9.

Figure 10 shows the displacement of the cavity bottom $z_{\text{piston}}(t)$ as a function of time equivalent to the above calculated tread penetration according to Eq.(14). The maximum equivalent displacement of the piston is 0.61 mm. The related maximum surface variation is about 2% and corresponds to the moment where the cavity is centered in the contact zone.

3.2. CFD method of resolution

The CFD model is implemented in the ANSYS Fluent code based on Finite Volume Method (FVM). Sliding and dynamic mesh fonctionalities [28] are used to handle the translational motion and rubber penetration in the cavity.

Figure 11 shows the 2D mesh of the CFD model. The fluid domain around the tyre is formed by a half-disc of 2.5 m radius divided into sub-domains according to their physical importance with respect to the flow. The most critical zones are located in front of and behind the contact zone and are finely meshed. The mesh is coarser when getting away from this area. The

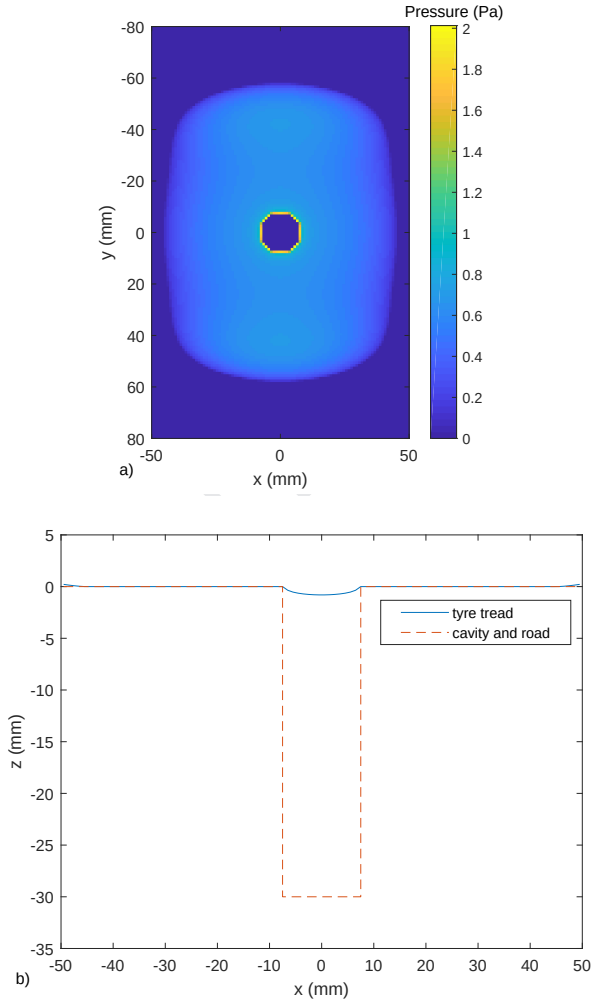

Figure 8: a) pressure distribution in the contact zone b) corresponding tyre tread penetration

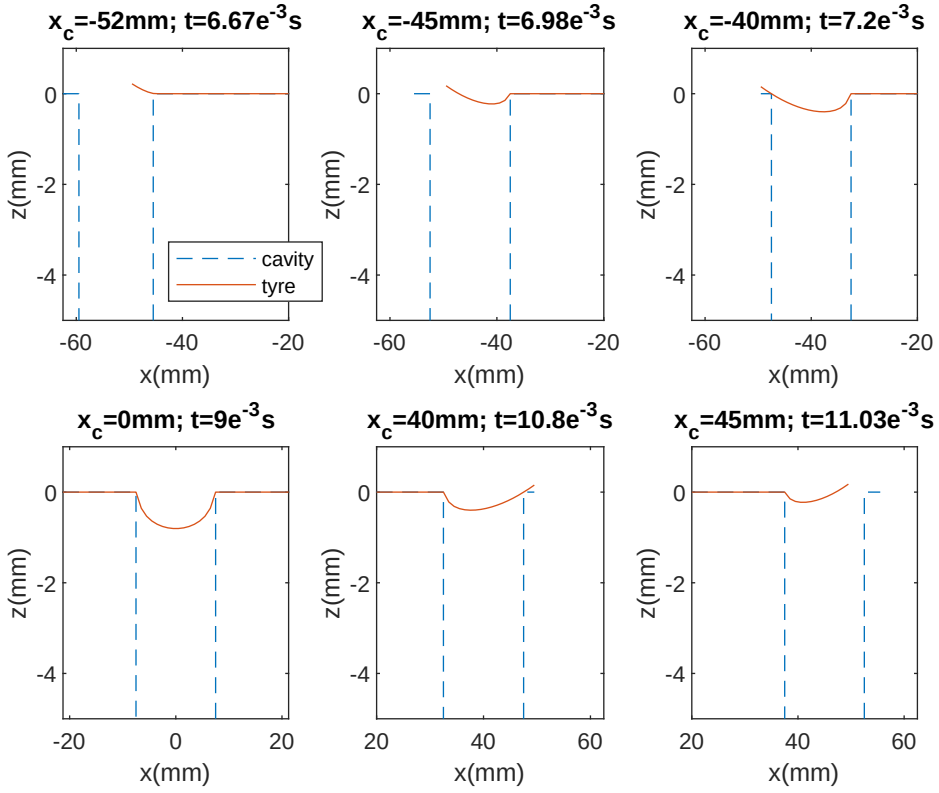

Figure 9: Tyre tread penetration for different locations of the cavity center relative to the wheel center (cavity of diameter 15 mm and depth 30 mm; rolling speed of 80 km/h)

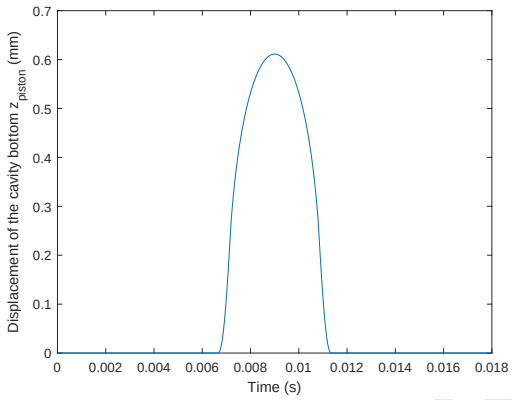

Figure 10: Equivalent displacement of the bottom of the cavity as a function of time (cavity of 15 mm in diameter and 30 mm deep; rolling speed 80 km/h)

fluid domain around the tyre is meshed according to the same principle and cell types as [13]. It is divided into six domains meshed from the coarsest to the finest near the contact zone.

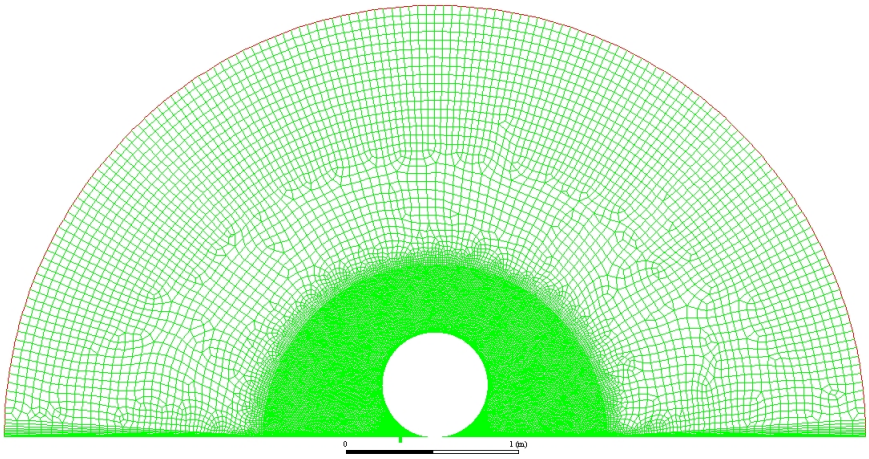

Figure 11: Mesh of the fluid domain adopted in the Fluent model

However, the smallest domain near the contact zone as well as the cavity are meshed differently in comparison with [13]: the spatial resolution according to x is fixed to 1 mm in order to fit with the mesh adopted in the contact model. The cavity of 15 mm in diameter is then meshed following 15

divisions according to x, by face mapping formed of quadrangular cells. The smallest domain of 10 mm in width is divided into 10 divisions (the mesh can be seen in Figure 12).

The air temperature at the outer boundary is fixed at 300 K (27 °C).

The translation velocity of the cavity and the road v is 22.2 m s^{-1} leading to an angular velocity of the tyre ω of 72.1 rad s^{-1}. Flow regime is determined by the Reynolds number Re defined as follows:

$$Re = \frac{\rho l V}{\mu} \tag{20}$$

where ρ, l, V, and μ are respectively the density, the characteristic linear dimension, the velocity and the dynamic viscosity. For the above conditions, these parameters are as follows: ρ=1.176 kg m^{-3}, l=1 m, V= 22.2 m s^{-1} and μ= 1.7894 x 10^{-5} kg m^{-1} s^{-1} resulting in a Reynolds number value Re = 1.46 x 10^6 higher than the turbulent regime limit ($Re > 5$ x 10^5).

The URANS models are the most appropriate to solve this type of flow. In fact, the flow is turbulent and controlled by the boundary layer phenomenon. An "improved" near-wall treatment is therefore necessary to resolve the flow in the inner zone of the boundary layer. In this study, the URANS $k-w$ SST turbulence model was considered as the most appropriate. This latter applies the $k-w$ model close to the wall and the $k-\epsilon$ model for cells away from the wall. The $k-w$ model stands on the following equations:

$$\frac{\partial(\rho k)}{\partial t} + \frac{\partial(\rho V_j k)}{\partial x_j} = \rho\tau_{ij}\frac{\partial V_i}{\partial x_j} - \beta^*\rho k\omega + \frac{\partial}{\partial x_j}\left[\left(\mu + \sigma^*\frac{\rho k}{\omega}\right)\frac{\partial k}{\partial x_j}\right] \tag{21}$$

$$\frac{\partial(\rho\omega)}{\partial t} + \frac{\partial(\rho V_j \omega)}{\partial x_j} = \alpha\frac{\omega}{k}\rho\tau_{ij}\frac{\partial V_i}{\partial x_j} - \beta\rho\omega^2 + \sigma_d\frac{\rho}{\omega}\frac{\partial k}{\partial x_j}\frac{\partial \omega}{\partial x_j} + \frac{\partial}{\partial x_j}\left[\left(\mu + \sigma\frac{\rho k}{\omega}\right)\frac{\partial \omega}{\partial x_j}\right] \tag{22}$$

where k is the specific turbulence kinetic energy, ω is the specific dissipation rate and β^*, σ^*, α, β, σ_d and σ are various closure coefficients whose values are given in [31]. The $k-\epsilon$ model stands on the following equations:

$$\frac{\partial(\rho k)}{\partial t} + \frac{\partial(\rho k V_i)}{\partial x_i} = \frac{\partial}{\partial x_j}\left[\frac{\mu_t}{\sigma_k}\frac{\partial k}{\partial x_j}\right] + 2\mu_t E_{ij}E_{ij} - \rho\epsilon \tag{23}$$

$$\frac{\partial(\rho \epsilon)}{\partial t} + \frac{\partial(\rho \epsilon V_i)}{\partial x_i} = \frac{\partial}{\partial x_j}\left[\frac{\mu_t}{\sigma_\epsilon}\frac{\partial \epsilon}{\partial x_j}\right] + C_{1\epsilon}\frac{\epsilon}{k}2\mu_t E_{ij}E_{ij} - C_{2\epsilon}\rho\frac{\epsilon^2}{k} \tag{24}$$

where μ_t is the eddy viscosity, E_{ij} are the components of the deformation rate, ϵ is the dissipation rate and σ_k, σ_ϵ, $C_{1\epsilon}$ and $C_{2\epsilon}$ are various closure coefficients whose values are given in [32].

The resolution of the problem is based on the PISO (Pressure-Implicit with Splitting of Operators) scheme. The pressure-based solver is used to solve the problem in two steps: first a stationary flow is considered for which no motion is assigned to the cavity. The solution obtained from the stationary simulation is used as initial condition for the unsteady problem. In a second step, the unsteady simulation is launched where the cavity moves with a translational velocity equal to the rolling speed v=22.2 m s^{-1}.

The Dynamic Mesh (DM) technique is activated in order to take into account the volume variation of the cavity. The calculated membrane penetration $z_m(x,t)$ or the equivalent piston displacement $z_{\text{piston}}(t)$ are assigned to the cavity by User Defined Functions (UDFs).

Besides the Sliding Interface (SI) fonctionality handling cavity translational motion, Fluent processes the Moving Deforming Mesh (MDM) or Dynamic Mesh (DM) in order to handle the topological changes of the domain during the simulation. Among the DM methods reported in [28], the smoothing technique is the most suitable for modeling the membrane and piston displacements. Smoothing enables to move the boundary and the inner nodes to absorb the movement of the moving domain without changing the number of nodes and their connectivity.

For the membrane method, the dynamic mesh is attributed to the upper face of the cavity assimilated to tyre tread surface when the cavity is travelling the contact area . For the piston method, it is attributed to the bottom of the cavity.

Fluent's User Defined Function (UDF) option is used to describe the movement prescribed to the moving surfaces (upper or lower face of the cavity depending on the method). For the membrane method, a function assigns at each time step and to each of the cavity upper wall nodes, a displacement corresponding to $z_m(x_i,t)$ by modifying its vertical position $z_i(t)$ according to the following equation:

$$z_i(t) = z_0 + z_m(x_i,t) \tag{25}$$

where z_0 is the vertical position of the road and $z_m(x_i,t)$ is obtained by the contact model.

Similarly, for the piston method, the UDF assigns to each of the cavity lower wall nodes, a displacement corresponding to $z_{\text{piston}}(t)$ by modifying its

vertical position $z_i(t)$ according to the following equation:

$$z_i(t) = z_0 - L_0 + z_{\text{piston}}(t) \tag{26}$$

where z_0 is the vertical position of the road, L_0 is the cavity depth ($L_0 = 0.03$ m) and $z_{\text{piston}}(t)$ is obtained by the contact model.

Figure 12 shows examples for the introduction of the volume variation by applying the dynamic mesh using both methods according to Eq.(25) and Eq.(26). Figure 12a illustrates the tyre tread penetration into the cavity according to the set of points $z_m(x,t)$. For the same moment of calculation, this penetration is equivalent to the cavity bottom displacement equal to $z_{\text{piston}}(t)$ (Figure 12b).

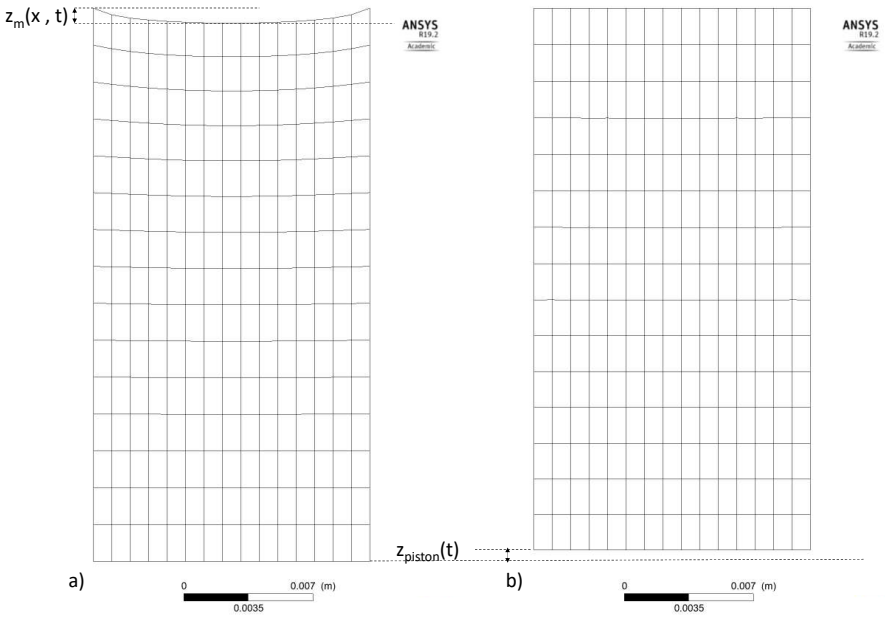

Figure 12: a) penetration of the tread into the cavity at the center of contact (membrane method); b) equivalent displacement of the cavity bottom (piston method)

3.3. Comparison of membrane and piston methods

The comparison between the membrane and the piston methods is based on the dynamic pressure p calculated at the bottom of the cavity during the tyre passage. Figure 13 shows the calculated dynamic air pressure at the cavity bottom taking into account the cavity volume variation caused by the tread penetration during the contact by the two tested methods: the membrane method (in solid green line) and the piston method (in dashed red line). The result without volume variation is also given (dotted blue curve) as a reference case. The latter shows a three-phase process: first a gradual air pressure increase in the cavity as the tyre approaches, then a constant over-pressure stage during the full cavity closure (with more or less pronounced cavity resonance), finally a pressure release with an Helmholtz resonance and pressure oscillations when the tyre leaves the cavity. These air compression and expansion with possible associated resonances characterize the air-pumping phenomenon at the tyre/road interface.

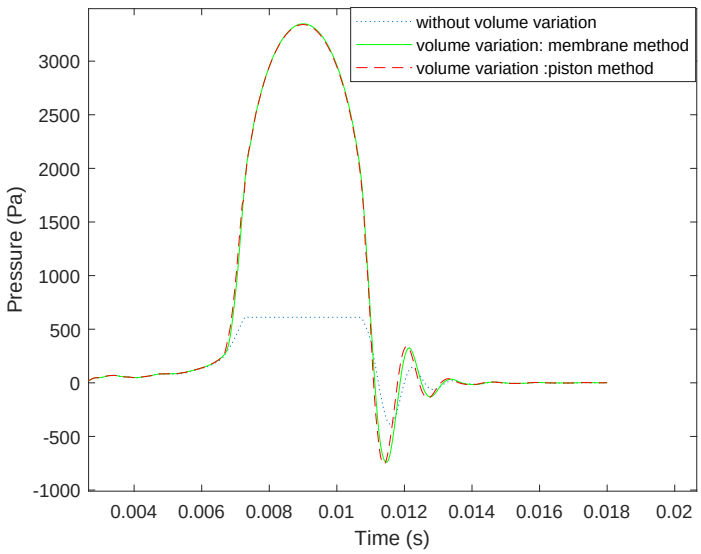

Figure 13: Variation of the dynamic air pressure at the bottom of the cavity due to volume variation modeled by membrane and piston methods and comparison with the case without volume variation (d=15 mm, L_0=30 mm, v=80 km/h)

First it can be observed that, in contrast to the reference case, the results with volume variation show an overpressure during the cavity closure with

a curved shape very similar to that of the volume variation drawn Figure 10. In that respect, once the cavity closed, the pressure variation is directly related to the volume variation and consequently to the contact model used for evaluating the tyre rubber penetration.

On the other hand, the curves obtained with volume variation by both implemented methods are very close to each other. The difference between the methods can be quantified by defining the error ϵ:

$$\epsilon = \left[\frac{\int_0^{T_s} [p(t) - p^*(t)]^2 dt}{\int_0^{T_s} [p^*(t)]^2 dt} \right]^{\frac{1}{2}} \tag{27}$$

where T_s is the duration of the signal and $p(t)$ and $p^*(t)$ are the calculated air pressure obtained respectively by the piston method and the membrane method at the same time t. ϵ is found equal to 3% when comparing all the signal points and equal to 0.2% when only comparing the maximum reached pressure. It can be deduced that the simplified piston method is equivalent to the membrane method in the case of a closed cylindrical cavity.

Thereby, this approach has proven to be efficient and representative of the air changing volume in the closed cavity: the air pressure fluctuations at the tyre/road interface calculated by the piston method are equivalent to those calculated by directly implementing the membrane displacement. Thus, the piston technique can be adopted to model the closed cavity volume variation during the rolling of the tyre and will be used in the following to study parameters influencing air-pumping.

4. Results

In this part, a parametric study is performed using the 2D piston method in order to evaluate the effect of volume variation and rolling speed on the dynamic air pressure at the cavity bottom. The pressure signal is also studied at the leading and trailing edges, respectively at 7cm forward and at 7cm behind the contact zone, in order to assess the pressure signals energy levels emitted at these locations. Simulations are also performed without volume variation.

The rolling speed is varied between 60 and 100 km/h with a step of 10 km/h and v_{ref}= 80 km/h is chosen as reference speed. The maximum volume variation (surface variation in this case) of the cavity obtained from the contact model is $\Delta S/S = 2$ %. The time step used for the simulations is now $\Delta t = 2.5\text{x}10^{-6}$ s.

4.1. Cavity grid dependency study

The influence of the mesh grid in the cavity on the calculation of the dynamic air pressure at the cavity bottom was first checked. Several squared meshes of the cavity have been tested according to Table 1, where Δ_x and Δ_y are the spatial resolutions of the cavity mesh according to x and y respectively. The finest mesh (Δ_x=Δ_y=0.1mm) is considered as the reference case and is about the size of the fluid domain nearest to the contact patch. The configuration (Δ_x=1mm; Δ_y=2mm) used for the comparison with the membrane method is also included in the study. The calculated pressure for the various meshes is presented in Figure 14. The error ϵ is quantified in Table 1 using Eq.(27) with $p^*(t)$ the pressure obtained in the reference case. It is shown that the difference compared to the finest mesh is low ($\epsilon \leq 2.5$ %) and the results are close for (Δ_x=Δ_y <1mm) or (Δ_x=1mm;Δ_y=2mm). This allows to conduct the following parametric study using the configuration of Section 3.2, i.e. (Δ_x=1mm; Δ_y=2mm), for which ϵ=2.5%.

Δ_x(mm)	0.1	0.25	0.5	1	2.5	3	5	1
Δ_y(mm)	0.1	0.25	0.5	1	2.5	3	5	2
d/Δ_x	150	60	30	15	6	5	3	15
L_0/Δ_y	300	120	60	30	12	10	6	15
ϵ(%)	—	1.4	2.3	4.6	7.2	8.4	9.0	2.5

Table 1: Cavity grid dependency study of the piston calculations and calculated error ϵ with respect to the finest mesh

4.2. Influence of volume variation

Figure 15 shows the temporal variation of the dynamic air pressures at the bottom of the cavity and at the leading edge and the trailing edge, with and without volume variation. It can be deduced that the volume variation of the cavity during contact has a significant impact on the air pressures at the contact interface. With regard to the pressure at the bottom of the cavity, the decrease in volume leads to an increase in the maximum pressure and in the amplitude and frequency of the pressure oscillations when the cavity opens. Likewise, the amplitude and frequency of pressure oscillations at the trailing edge increase with decreasing cavity volume. With regard to the pressure at the leading edge, there is a decrease in the amplitude of the

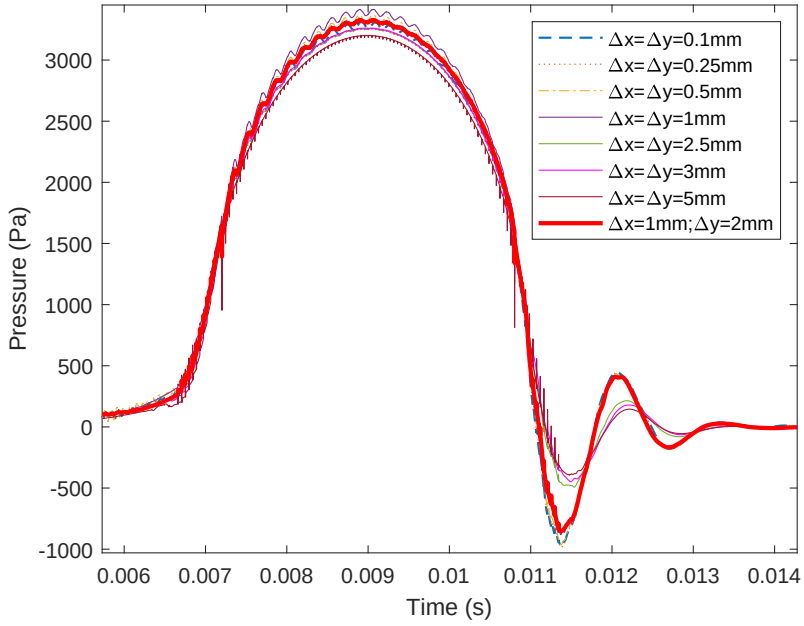

Figure 14: Dynamic air pressure at the cavity bottom for different mesh resolutions Δ_x and Δ_y of the cavity grid (d= 15 mm, L_0=30 mm, v=80 km/h)

pressure wave peak released at the total closure of the cavity but an increase in amplitude at its closure.

On the other hand, the plateau phase of the signal without volume change is replaced, in the signal with volume variation, by a pressure peak similar to the shape of the volume variation obtained by the contact model and coupled in the CFD model (refer to Figure 10). The pressure signal without volume variation has in fact a plateau phase with a cavity resonance when it is completely closed. Considering Figures 15b and 15c, it is worth noting that a similar behaviour was found by Eisenblaetter [16] at the leading and trailing edges of a rotating tyre equipped with a cylindrical cavity similar to the road cavity considered in the present paper. The signal at the leading edge is characterized by a sharp peak just before the full closure of the cavity, while at the trailing edge the signal consists of damped oscillations, namely Helmholtz resonance occurring when the cavity opens.

4.3. Speed influence on the maximum average pressure at the cavity bottom

The temporal variation of the pressure at the cavity bottom at the different rolling speeds is given in Figure 16a for the cases without volume variation and in Figure 16b for the cases with volume variation. In both cases, the maximum pressure reached at the bottom of the cavity during the contact increases with the rolling speed.

4.4. Speed influence on the pressure signal energy level

The transient signals at the leading and trailing edges are used to assess the corresponding pressure signal energy level N emitted in front of and behind the contact zone according to the following relation:

$$N = 10 \log_{10} \int_{t_i}^{t_f} p^2(t) dt \tag{28}$$

where p is the pressure and $[t_i, t_f]$ is the time integration interval.

For the leading edge, t_i and t_f are chosen where the difference between the signals with and without volume variation is the most important (Figure 17a). An offset is to be noticed in the pressure signal. The integration time is chosen constant among all tested rolling speeds. It corresponds to the one identified for the lowest rolling speed (60 km/h).

For the trailing edge, t_i corresponds to the cavity opening start time and t_f corresponds to the oscillations end time (Figure 17b). Despite an offset

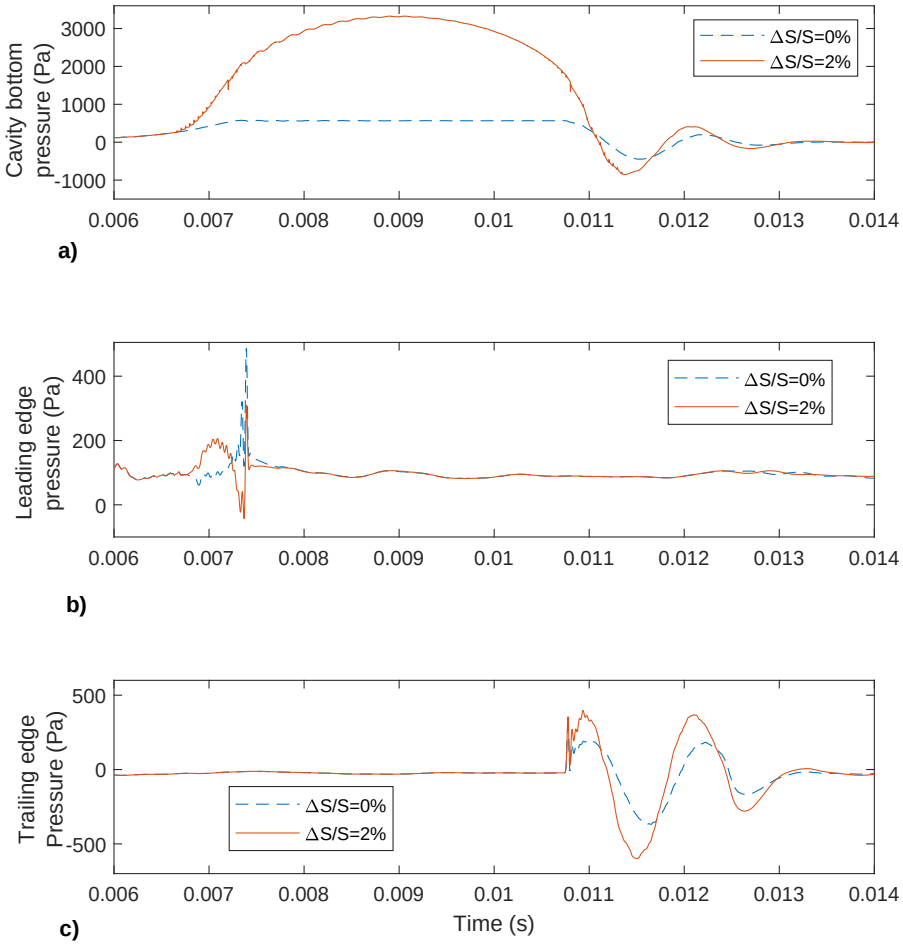

Figure 15: Influence of volume variation on the calculated air pressure a) at the cavity bottom b) at the leading edge c) at the trailing edge (rolling speed at 80 km/h)

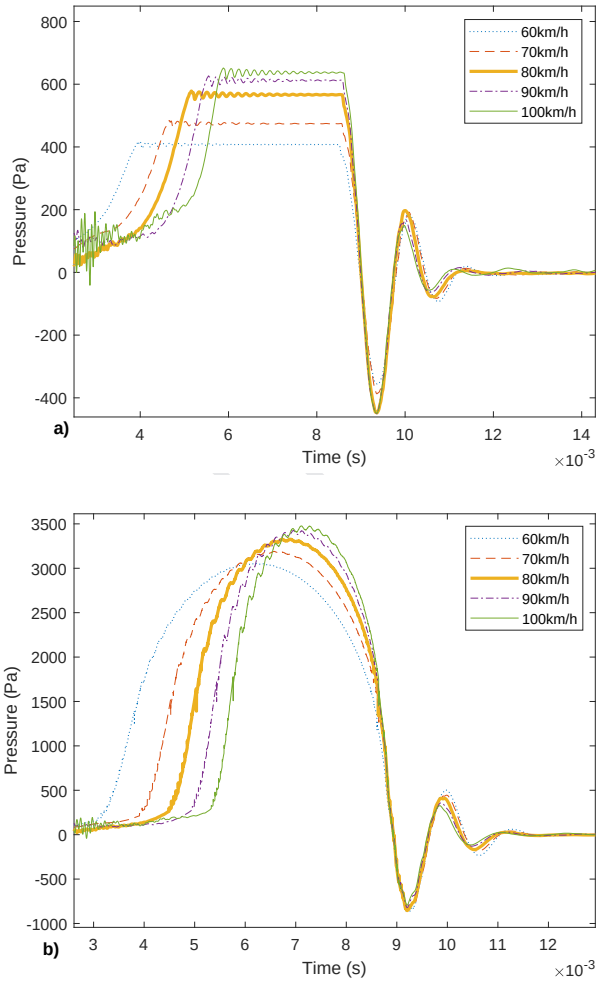

Figure 16: Speed influence on the calculated air pressure at the cavity bottom a) without volume variation b) with volume variation

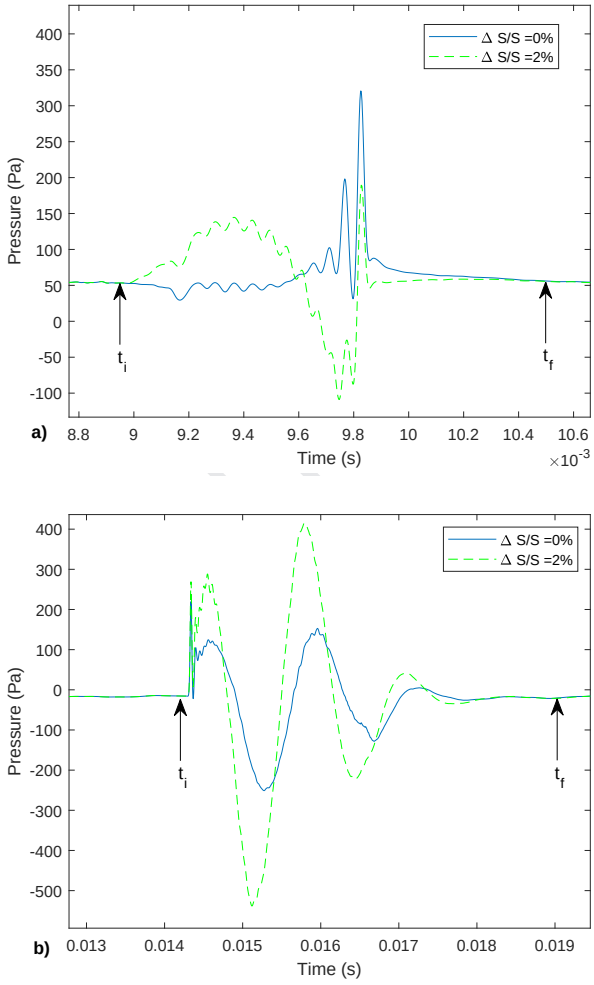

Figure 17: Pressure signals definition for a rolling speed of 60 km/h a) at the leading edge b) at the trailing edge

smaller than at the leading edge, a constant integration time is chosen that corresponds to that identified for 60 km/h again.

Energy levels at the leading edge and at the trailing edge during the passage of the tyre over the cylindrical cavity are calculated as a function of the rolling speed and compared to the case without volume variation in Figure 18.

Volume variation has a greater effect on the energy level at the trailing edge than on the leading edge. In fact, energy level at the trailing edge increases with volume variation. However, this latter influences the dynamic air pressure at the leading edge without having a significant effect on the related energy level.

On the other side, energy level at the leading edge increases with increasing speed with and without considering the volume variation. However, rolling speed has no influence on the energy level at the trailing edge when considering the cavity volume variation. When this latter is not considered, energy level at the trailing edge increases with increasing speed.

Speed exponent k characterizing the linear relationship between signal energy and rolling speed raised to power k satisfies the following equation between energy level and logarithm of rolling speed:

$$N(v) = 10log_{10}(v/v_{\text{ref}})^k + N(v_{ref}) \tag{29}$$

A linear regression is used to determine k and $N(v_{ref})$ values. Figure 18 illustrates the correlation between N and v according to Eq.(29). Table 2 summarizes the values of k and $N(v_{ref})$ thus found for the energy levels emitted at the leading and trailing edges for cases with and without volume variation, as well as the correlation coefficient of determination R^2.

	k	$N(v_{ref})$	R^2
$\Delta S/S = 0\%$ (leading edge)	3.45	14.13	0.99
$\Delta S/S = 2\%$ (leading edge)	2.87	14.07	0.99
$\Delta S/S = 0\%$ (trailing edge)	1.34	18.19	0.86
$\Delta S/S = 2\%$ (trailing edge)	0.13	22.9	0.23

Table 2: Calculated speed coefficient k, reference energy level $N(v_{ref})$ and coefficient of determination R^2.

R^2 is close to 1 for the leading edge (with and without volume variation) as well as for the trailing edge without volume variation, indicating a good

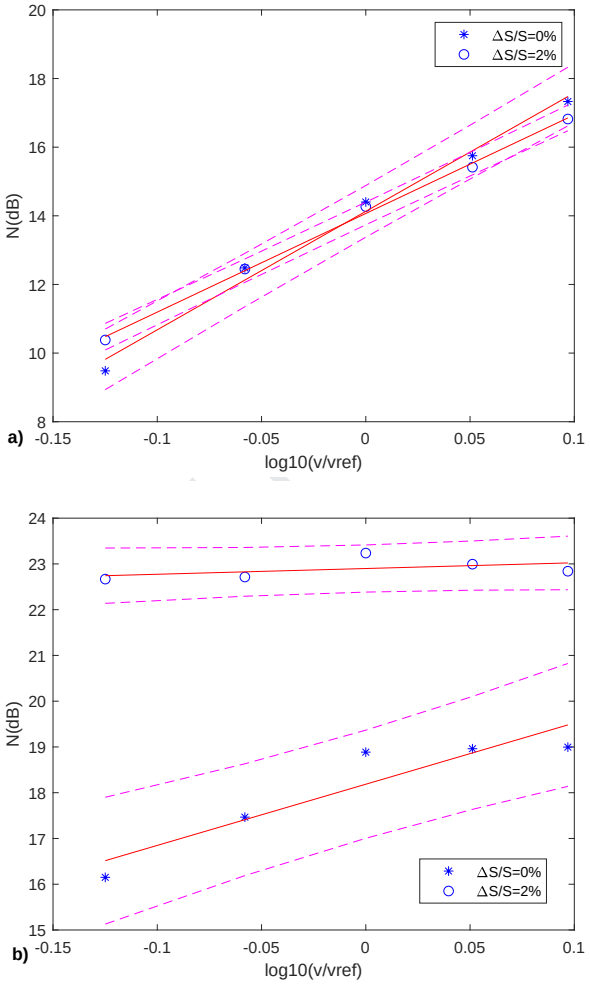

Figure 18: Energy level as a function of rolling speed with and without volume variation a) at the leading edge b) at the trailing edge. (—) best fit linear regression line, (...) 95% prediction interval.

prediction quality of the linear regression. However, since the rolling speed has no effect on the energy level emitted at the trailing edge in the case with volume variation, R^2 is very low. Comparing with literature, the results at the leading and trailing edges for both cases, with and without volume variation, are in agreement with [9] where k appears lower than 4. It is also worth noting that in Conte's PhD [33] the speed exponent k of the signal energy was 3 at the leading edge and 2 at the trailing edge, which is close to the results of Table 2 for the case without volume variation ($\Delta S/S$ =0 %). Even though a tyre cavity instead of a road cavity was considered in Eisenblaetter's work [16], and the calculations in the present paper are in 2D, it is interesting to compare the speed dependency of the signals in both cases. In [16], at the leading edge the peak amplitudes was found to be proportional to the square of the velocity, i.e. a speed exponent of $k = 4$ was found contrary to $k = 2.87$ found in Table 2 for $\Delta S/S = 2\%$. However, at the trailing edge no proportionality was found in [16] which agrees with Table 2 where $k = 0.13$ for $\Delta S/S = 2\%$.

5. Conclusions

This paper highlights the influence of volume variation in a road cavity on the dynamic air pressure at the tyre/road interface during rolling of a slick tyre. This volume variation is due to the tyre tread penetration into the cavity. The numerical method used is based on a contact model coupled with a CFD model using the Fluent solver.

A simplified piston method was proposed to model the volume variation by considering the piston-like motion of the cavity bottom. The latter moves vertically upward as the cavity closes and then symmetrically down as it opens. This technique was found equivalent to the direct tyre tread penetration into the cavity calculated by the contact model. Furthermore, a parametric study was conducted using the piston method in order to evaluate the influence of the volume variation and the rolling speed on the air pressure at the bottom of the cavity, at the leading edge and at the trailing edge. The pressure signal energy level emitted at these locations was also assessed.

Volume variation increases the over-pressure at the bottom of the cavity reached during its complete closure. The maximum pressure increases with the increase of rolling speed in both cases (with and without volume variation). Signal energy level at the leading edge is weakly influenced by

volume variation, while at the rear it increases with volume variation. Moreover, signal energy level increases with the rolling speed at the leading edge for both cases with and without volume variation, as well as for the trailing edge without considering the volume variation. However, when the latter is considered at the trailing edge, it has no influence on the related signal energy level. The speed exponent linking energy level with the rolling speed appeared to be lower than 4 at the front edge and the rear edge.

Considering the efficiency of the piston method, it would therefore be interesting to perform CFD simulations in 3D in order to carry out comparisons with related measurements and to further highlight the influence of volume variation on aerodynamic sources in more complex configurations. Moreover, the cylindrical cavity could be replaced by a transverse groove included in the road surface in order to deepen the influence of volume variation in such a configuration and to compare the results with the case without volume variation [34]. Similarities with some previous works (e.g. [35, 36]) dealing with a deformed tyre groove rolling on a smooth surface could also be investigated.

Acknowledgements

This work has been jointly funded by the Région Pays de la Loire and IFSTTAR.

"Declarations of interest: none"

[1] WHO, Environmental Noise Guidelines for the European Region, Tech. rep., World Health Organization - Regional Office for Europe (Oct. 2018).

[2] J.-F. Hamet, F. Besnard, S. Doisy, J. Lelong, E. le Duc, New vehicle noise emission for French traffic noise prediction, Applied Acoustics 71 (9) (2010) 861–869 (Sep. 2010).

[3] U. Sandberg, G. Descornet, Road surface influence on tire/road noise, in: Proceedings of Internoise 1980, Miami, Florida, 1980, pp. 1–16 (1980).

[4] M. Heckl, Tyre noise generation, Wear 113 (1) (1986) 157–170 (Dec. 1986).

[5] U. Sandberg, J. A. Ejsmont, Tyre/road noise reference book, Informex Ejsmont & Sandberg, 2002 (2002).

[6] W. Kropp, F.-X. Bécot, S. Barrelet, On the Sound Radiation from Tyres, Acta Acustica united with Acustica 86 (5) (2000) 769–779 (Sep. 2000).

[7] R. A. G. Graf, C. Y. Kuo, A. P. Dowling, W. R. Graham, On the horn effect of a tyre/road interface, part I: Experiment and computation, Journal of Sound and Vibration 256 (3) (2002) 417–431 (Sep. 2002).

[8] A. Kuijpers, G. Van Blokland, Tyre/road noise models in the last two decades: a critical evaluation, in: Internoise and Noisecon Congress and Conference Proceedings, Vol. 2001, Institute of Noise Control Engineering, The Hague, Holland, 2001, pp. 2494–2499 (2001).

[9] A. Kuijpers, Further analysis of the Sperenberg data, Towards a better understanding of processes influencing tyre/road noise, Tech. rep., Hertogenbosch : M+P Raadgevende Ingenieurs (2001).

[10] J. Winroth, W. Kropp, C. Hoever, T. Beckenbauer, M. Männel, Investigating generation mechanisms of tyre/road noise by speed exponent analysis, Applied Acoustics 115 (2017) 101–108 (Jan. 2017).

[11] T. Li, R. Burdisso, C. Sandu, Literature review of models on tire-pavement interaction noise, Journal of Sound and Vibration 420 (2018) 357–445 (Apr. 2018).

[12] J.-F. Hamet, C. Deffayet, M.-A. Pallas, Air-pumping phenomena in road cavities, in: INTROC 90 - International Tire/Road Noise Conference 1990, Gothenburg, Sweden, 1990, pp. 29–35 (1990).

[13] F. Conte, P. Jean, CFD modelling of air compression and release in road cavities during tyre/road interaction, in: Proc. Euronoise 2006, Tampere, Finland, 2006, p. 6 p (Jun. 2006).

[14] R. Pinnington, A compressible fluid model for opening and closing dynamics, Tech. Rep. ITARI Deliverable 2.1b, Institute of Sound and Vibration Research, University of Southampton, Southampton (United Kingdom) (2007).

[15] J. Ejsmont, U. Sandberg, S. Taryma, Influence of Tread Pattern on Tire/Road Noise, SAE Technical Paper 841238:5632-5640, SAE International, Warrendale, PA (Sep. 1984).

[16] J. Eisenblaetter, Experimental investigation of air related tyre/road noise mechanisms, PhD Thesis, Loughborough University (2008).

[17] R. E. Hayden, Roadside noise from the interaction of a rolling tire with the road Surface, The Journal of the Acoustical Society of America 50 (1A) (1971) 113–113 (Jul. 1971).

[18] M. J. Gagen, Novel acoustic sources from squeezed cavities in car tires, The Journal of the Acoustical Society of America 106 (2) (1999) 794–801 (Jul. 1999).

[19] N. A. Nilsson, Possible methods of reducing external tire noise, in: Proc. of the International Tire Noise Conference 1979, Stockholm, 1979 (1979).

[20] S. Kim, W. Jeong, Y. Park, S. Lee, Prediction method for tire air-pumping noise using a hybrid technique, The Journal of the Acoustical Society of America 119 (6) (2006) 3799–3812 (Jun. 2006).

[21] C. Fabrizi, Computational Aeroacoustic Analysis of a Rolling Tire, Tire Science and Technology 44 (4) (2016) 262–279 (Oct. 2016).

[22] P. Gautam, A. J. Chandy, Numerical Investigation of the Air Pumping Noise Generation Mechanism in Tire Grooves, Journal of Vibration and Acoustics 138 (5) (2016) 051002–051002–8 (May 2016).

[23] P. Gautam, A. J. Chandy, A Three-Dimensional Numerical Investigation of Air Pumping Noise Generation in Tires, Journal of Vibration and Acoustics 138 (6) (2016) 061005–061005–11 (Dec. 2016).

[24] D. Ronneberger, Towards a quantitative prediction of Tire/Road Noise, in: Workshop on rolling noise generation, Berlin, Germany, 1989, pp. 219–234 (1989).

[25] J.-F. Hamet, C. Deffayet, M.-A. Pallas, Phénomènes d'air-pumping dans le bruit de contact pneumatique/chaussée. Cas d'une cavité aménagée dans la chaussée [Air-pumping phenomena in Tire/Road noise. Case of a road cavity], Rapport INRETS 132, INRETS, France (Dec. 1990).

[26] M. Bou Leba Bassil, J. Cesbron, P. Klein, CFD modeling of pressure variation in a road cavity with volume variation, in: 23rd International Congress on Acoustics, EEA, ICA, DEGA, Aachen, Germany, 2019, pp. p. 506–513 (Sep. 2019).

[27] J. Boussinesq, Application des potentiels à l'étude de l'équilibre et du mouvement des solides élastiques [Application of potentials to the study of the equilibrium and the movement of elastic solids], Gauthier-Villars, 1885 (1885).

[28] ANSYS Inc, ANSYS FLUENT 12.0 User's Guide (2013).

[29] K.-L. Johnson, Contact Mechanics, Cambridge University Press (CUP), 1985 (1985).

[30] J. Cesbron, H.-P. Yin, Contact analysis of road aggregate with friction using a direct numerical method, Wear 268 (5-6) (2010) 686–692 (2010).

[31] D. C. Wilcox, Formulation of the k-w Turbulence Model Revisited, AIAA Journal 46 (11) (2008) 2823–2838 (2008). doi:10.2514/1.36541.

[32] H. K. Versteeg, W. Malalasekera, An Introduction to Computational Fluid Dynamics: The Finite Volume Method, Pearson Education, 2007 (2007).

[33] F. Conte, Modélisation CFD du phénomène acoustique de pompage d'air dans un contact pneumatique / chaussée [CFD modeling of the acoustic phenomenon of air pumping in a tyre/road contact], PhD Thesis, Lyon, INSA (Jan. 2008).

[34] F. Conte, P. Klein, 3D CFD modelling of air pumping noise from road cavities with constant volume, in: Internoise 2013 : 42nd International Congress and Exposition on Noise Control Engineering, Autriche, 2013, p. 10 p (Jan. 2013).

[35] P. Gautam, Y. Azizi, A. Chandy, An experimental and computational investigation of air-borne noise generation mechanisms in tires, Journal of Vibration and Control 25 (3) (2018) 529–537 (Jul. 2018).

[36] K. Takami, T. Furukawa, Study of tire noise characteristics with high-resolution synchronous images, in: Proceedings of EURONOISE, Maastricht,Netherlands, 2015, pp. 2113–2118 (2015).